The Astrophysical Journal, 995:193 (9pp), 2025 December 20 https://doi.org/10.3847/1538-4357/ae2250

The ALMA-QUARKS Survey: Evidence of a Candidate High-mass Prestellar Core Aside a Bright-rimmed Cloud IRAS 18290-0924

Dongting Yang[1], Hong-Li Liu[1], Sheng-li Qin[1], Tie Liu[2], Anandmayee Tej[3], Siju Zhang[4], Xunchuan Liu[2], Fengwei Xu[5,6], Guido Garay[7,8], Lei Zhu[8], Patricio Sanhueza[9], Xiaofeng Mai[10,11], Wenyu Jiao[2], Paul F. Goldsmith[12], Sami Dib[13], Pablo García[14,15], Di Li[16], Jinhua He[4,8,17], A. Y. Yang[18,19], Prasanta Gorai[20,21], Suinan Zhang[2], Yankun Zhang[2], Jianjun Zhou[22], Mika Juvela[23], James O. Chibueze[24,25], Chang Won Lee[26,27], Jihye Hwang[26], Leonardo Bronfman[7], Xindi Tang[22], Archana Soam[28], Tapas Baug[29], Yichen Zhang[30], Swagat Ranjan Das[7], L. K. Dewangan[31], and L. Viktor Tóth[32,33]

[1] School of Physics and Astronomy, Yunnan University, Kunming 650091, People's Republic of China; hongliliu2012@gmail.com, qin@ynu.edu.cn
[2] Shanghai Astronomical Observatory, Chinese Academy of Sciences, 80 Nandan Road, Shanghai 200030, People's Republic of China; liutie@shao.ac.cn
[3] Indian Institute of Space Science and Technology, Thiruvananthapuram 695 547, Kerala, India; tej@iist.ac.in
[4] Departamento de Astronomía, Universidad de Chile, Las Condes, 7591245 Santiago, Chile
[5] Kavli Institute for Astronomy and Astrophysics, Peking University, 5 Yiheyuan Road, Haidian District, Beijing 100871, People's Republic of China
[6] Department of Astronomy, Peking University, Beijing 100871, People's Republic of China
[7] Departamento de Astronomía, Universidad de Chile, Casilla 36-D, Santiago, Chile
[8] Chinese Academy of Sciences South America Center for Astronomy, National Astronomical Observatories, Chinese Academy of Sciences, Beijing 100101, People's Republic of China
[9] Department of Astronomy, School of Science, The University of Tokyo, 7-3-1 Hongo, Bunkyo, Tokyo 113-0033, Japan
[10] Shanghai Astronomical Observatory, Chinese Academy of Sciences, Shanghai 200030, People's Republic of China
[11] School of Astronomy and Space Sciences, University of Chinese Academy of Sciences, No. 19A Yuquan Road, Beijing 100049, People's Republic of China
[12] Jet Propulsion Laboratory, California Institute of Technology, 4800 Oak Grove Drive, Pasadena, CA 91109, USA
[13] Max Planck Institute for Astronomy, Königstuhl 17, D-69117 Heidelberg, Germany
[14] Chinese Academy of Sciences South America Center for Astronomy, National Astronomical Observatories, CAS, Beijing 100101, People's Republic of China
[15] Instituto de Astronomía, Universidad Católica del Norte, Av. Angamos 0610, Antofagasta, Chile
[16] New Cornerstone Science Laboratory, Department of Astronomy, Tsinghua University, Beijing 100084, People's Republic of China
[17] Yunnan Observatories, Chinese Academy of Sciences, Kunming 650216, Yunnan, People's Republic of China
[18] National Astronomical Observatories, Chinese Academy of Sciences, Beijing 100101, People's Republic of China
[19] Key Laboratory of Radio Astronomy and Technology, Chinese Academy of Sciences, A20 Datun Road, Chaoyang District, Beijing 100101, People's Republic of China
[20] Rosseland Centre for Solar Physics, University of Oslo, P.O. Box 1029 Blindern, 0315 Oslo, Norway
[21] Institute of Theoretical Astrophysics, University of Oslo, P.O. Box 1029 Blindern, 0315 Oslo, Norway
[22] Xinjiang Astronomical Observatory, Chinese Academy of Sciences, 150 Science 1-Street, Urumqi, Xinjiang 830011, People's Republic of China
[23] Department of Physics, P.O. Box 64, FI- 00014, University of Helsinki, Finland
[24] Department of Mathematical Sciences, University of South Africa, Cnr Christian de Wet Road and Pioneer Avenue, Florida Park, 1709, Roodepoort, South Africa
[25] Department of Physics and Astronomy, Faculty of Physical Sciences, University of Nigeria, Carver Building, 1 University Road, Nsukka 410001, Nigeria
[26] Korea Astronomy and Space Science Institute, 776 Daedeokdae-ro, Yuseong-gu, Daejeon 34055, Republic of Korea
[27] University of Science and Technology, Korea (UST), 217 Gajeong-ro, Yuseong-gu, Daejeon 34113, Republic of Korea
[28] Indian Institute of Astrophysics, II Block, Koramangala, Bengaluru 560034, India
[29] S. N. Bose National Centre for Basic Sciences, Block-JD, Sector-III, Salt Lake City, Kolkata 700106, India
[30] Department of Astronomy, Shanghai Jiao Tong University, 800 Dongchuan Road, Minhang, Shanghai 200240, People's Republic of China
[31] Astronomy & Astrophysics Division, Physical Research Laboratory, Navrangpura, Ahmedabad 380009, India
[32] Institute of Physics and Astronomy, Eötvös Loránd University, Pázmány Péter sétány 1/A, H-1117 Budapest, Hungary
[33] Faculty of Science and Technology, University of Debrecen, H-4032 Debrecen, Hungary

Received 2025 September 10; revised 2025 November 12; accepted 2025 November 18; published 2025 December 16

Abstract

Although frequently reported in observations, the definitive confirmation of high-mass prestellar cores has remained elusive, presenting a persistent challenge in star formation studies. Using two-band observational data from the 3 mm ATOMS and 1.3 mm QUARKS surveys, we report a high-mass prestellar core candidate, C2, located on the side of the bright-rimmed cloud IRAS 18290-0924. The C2 core identified from the 3 mm continuum data of the ATOMS survey ($\sim 2''$, $\sim$10,000 au at 5.3 kpc) has a mass ranging from 27 to 68 $M_{\odot}$ for temperatures 10–22 K within a radius of $\sim$2800 au. The highest-resolution ($\sim 0''.3$, $\sim$1500 au) observations of this source presented to date from the QUARKS survey reveal no evidence of further fragmentation. Further analysis of a total $\sim$10 GHz bandwidth of molecular line survey does not find star formation activity (e.g., outflows and ionized gas) associated with the core, with a few molecular lines of cold gas detected only. Additionally, virial analysis indicates the C2 core is gravitationally bound ($\alpha_{\rm vir} \sim 0.1-0.3$) and thus could be undergoing collapse toward star formation. These results strongly establish a candidate for a high-mass prestellar core, contributing to the very limited number of such sources known to date.

Unified Astronomy Thesaurus concepts: Dust continuum emission (412); Interstellar medium (847); Sub-millimeter astronomy (1647); Molecular clouds (1072); Star forming regions (1565); Massive stars (732)

1. Introduction

Understanding star formation requires tracing the evolution of molecular gas from its earliest prestellar phase to the formation of protostars (P. Andre et al. 2000). For high-mass

stars, which typically form in clusters, their far distances, short evolutionary timescales, and intense stellar feedback make it particularly challenging to directly observe the formation process (C. J. Lada & E. A. Lada 2003; Q. Zhang et al. 2009). Despite extensive observational and theoretical research over the past few decades, the exact mechanisms driving high-mass star formation remain uncertain (F. Motte et al. 2018).

Currently, the two widely accepted models of high-mass star formation are the "turbulent core accretion" model (C. F. McKee & J. C. Tan 2003) and the "competitive accretion" model (I. A. Bonnell et al. 2001). The former posits the existence of a preassembled massive gas reservoir within a clump, which contains the final mass required to form a high-mass star. This structure, referred to as a massive prestellar core, maintains stability against collapse due to support mechanisms that include turbulence and magnetic fields. In contrast, in the "competitive accretion" model, the massive gas clumps initially fragment into thermal-Jeans-like low-mass cores. Subsequently, these cores competitively accrete gas from the clump-scale reservoir. Here, the more massive cores located deeper in the gravitational potential well of the clump exhibit larger accretion efficiency and accelerated mass growth. Furthermore, accretion flows from filamentary structures associated with hub-filament systems enable additional gas mass flow into the cores from larger scales (>1 pc), facilitating the more efficient and rapid formation of massive stars in the central hubs (e.g., N. Peretto et al. 2013; E. Vázquez-Semadeni et al. 2019; P. Padoan et al. 2020; D. Yang et al. 2023; S. R. Das et al. 2024).

Extensive observational investigations from the Submillimeter Array (SMA), Northern Extended Millimater Array (NOEMA), and Atacama Large Millimeter/submillimeter Array (ALMA) revealed that massive gas clumps predominantly fragment into low-mass cores, which subsequently accrete gas and grow mass to form massive stars (Q. Zhang et al. 2015; H. Beuther et al. 2018; P. Sanhueza et al. 2019; B. E. Svoboda et al. 2019; S. Zhang et al. 2021; K. Morii et al. 2024; A. Coletta et al. 2025). In comparison, case studies as well as large-sample statistical analysis have not found conclusive evidence for the existence of massive prestellar cores (e.g., F. Motte et al. 2007; S. Bontemps et al. 2010; J. C. Tan et al. 2013; F. Louvet et al. 2019; W. Jiao et al. 2023; K. Morii et al. 2023).

Based on numerous observational results, F. Motte et al. (2018) proposed an evolutionary scenario for massive star formation that excludes such high-mass prestellar cores. However, the detection of a limited number of massive prestellar core candidates ($\gtrsim 16 M_{\odot}$; e.g., A. Duarte-Cabral et al. 2013; C. J. Cyganowski et al. 2014; K. Wang et al. 2014; A. T. Barnes et al. 2023; X. Mai et al. 2024; F. Xu et al. 2024a; M. Valeille-Manet et al. 2025) continues to sustain the debate about massive star formation mechanisms. The detection of specific molecular lines distinguishes the prestellar or protostellar nature of dense cores (e.g., P. Sanhueza et al. 2019; D. Yang et al. 2025), as star formation activity within protostellar cores increases the ambient temperature, thus releasing complex organic molecules (COMs; e.g., CH_3OH) from grain mantles into the gas phase, which then become observable (T. Gerner et al. 2014). Reliable identification of high-mass prestellar cores is challenging without a broad frequency range survey of molecular lines (e.g., A. Duarte-Cabral et al. 2013; K. Wang et al. 2014; T. Nony et al. 2018; J. Molet et al. 2019; M. Valeille-Manet et al. 2025). In addition, their interpretation is further complicated by the ambiguous absence of outflows and the observed presence of fragmentation (A. Duarte-Cabral et al. 2013; X. Mai et al. 2024).

The search for high-mass prestellar cores has primarily focused on infrared-dark environments, as only these regions are believed to harbor massive cloud cores in their earliest evolutionary stages (e.g., J. C. Tan et al. 2013; P. Sanhueza et al. 2017; F. Motte et al. 2018). However, recent studies suggest that massive prestellar cores may also exist within infrared-bright environments (e.g., P. Sanhueza et al. 2019; F. Xu et al. 2024a). This is likely due to elevated temperatures and heightened turbulence in these regions. The increased temperature raises the Jeans mass, which in turn facilitates the formation of high-mass prestellar cores, particularly when combined with the additional support provided by magnetic fields.

Bright-rimmed clouds (BRCs) constitute a distinct class of infrared-bright star-forming environments (K. Sugitani et al. 1991; K. Sugitani & K. Ogura 1994). They are characterized by an ionized surface on one side, created by intense ultraviolet radiation from nearby OB stars, which forms an overpressured ionized boundary layer. This boundary layer can be traced via free–free emission or radio recombination lines. Investigations of massive star formation in BRCs, particularly those focusing on embedded high-mass prestellar cores, remain scarce. Thus, identifying such cores within BRCs is crucial for constraining models of massive star formation.

The target of this study is a massive star formation region associated with the BRC, IRAS 18290-0924 (hereafter I18290; see Figure 1) with estimated clump mass $\sim 1500\, M_{\odot}$ and luminosity $\sim 10^4\, L_{\odot}$ (J. S. Urquhart et al. 2018; T. Liu et al. 2020). Located at a kinematic distance of $\sim 5.34 \pm 0.5$ kpc (X. Lu et al. 2014; J. S. Urquhart et al. 2018; P. Mège et al. 2021), this region hosts dense cores that display a small-scale (<1 pc) age sequence aligned with the direction of ionization, indicative of subsequent star formation triggered by radiation-driven implosion (S. Zhang et al. 2023). Among them, the C2 core, situated farthest from the bright rim, has been proposed as a high-mass prestellar core candidate (S. Zhang et al. 2023). In this work, we utilize ALMA two-band observations (see Section 2) to perform a comprehensive analysis of the C2 core with the aim of assessing its evolutionary stage and evaluating its candidacy as a high-mass prestellar core.

2. Observations

The I18290 region has been observed both in the ALMA Three-millimeter Observations of Massive Star-forming regions (ATOMS; Project ID: 2019.1.00685.S; T. Liu et al. 2020; H.-L. Liu et al. 2021) survey and the Querying Underlying mechanisms of massive star formation with ALMA-Resolved gas Kinematics and Structures (QUARKS; Project ID: 2021.1.00095.S; X. Liu et al. 2024; F. Xu et al. 2024b; D. Yang et al. 2025) survey.

Observations for the ATOMS survey were conducted using ALMA 7 m Atacama Compact Array (ACA) and the 12 m arrays at Band 3 (~3 mm), targeting 146 massive star-forming protocluster clumps. Further details regarding the ATOMS survey are available in T. Liu et al. (2020). ACA and 12 m array data from the ATOMS survey were combined to produce continuum and images and line cubes, resulting in an angular resolution ~2″ for continuum emission. For I18290, the combined continuum data have rms noise ($\sigma_{3\,\mathrm{mm}}$) ~0.1 mJy beam^{-1}. For line cubes of the ATOMS survey, eight spectral windows (SPWs) were configured, including six high-spectral-resolution SPWs

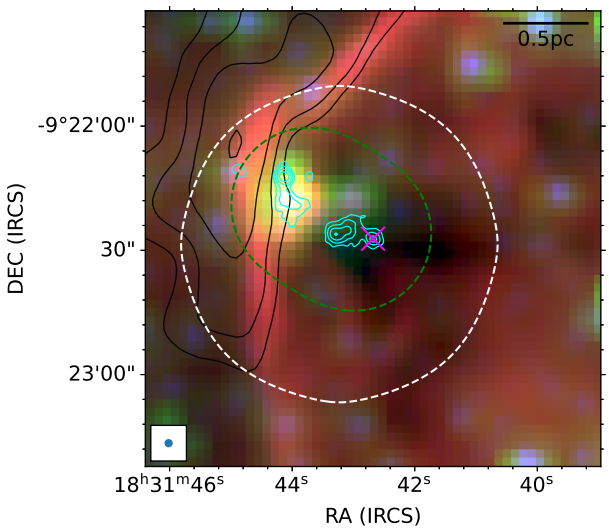

Figure 1. Three-color image of Spitzer 8 μm (red), 4.5 μm (green), and 3.6 μm (blue) of the region associated with I18290. The black contours represent the 1.28 GHz MeerKAT emission. The white and green dashed circles show the field of view of the ATOMS and QUARKS survey, respectively. ATOMS 3 mm dust continuum emission is shown as the cyan contours, with levels starting at $3\sigma_{3\ \mathrm{mm}}$ ($\sim$0.1 mJy beam^{-1}) and increasing as [6, 12, 24, 48] $\times\ \sigma_{3\ \mathrm{mm}}$. The purple cross symbol shows the location of Core 2 (S. Zhang et al. 2023). The synthesized beam size of the ATOMS survey and the 0.5 pc scale bar are shown in the lower left corner and upper right corner, respectively.

($\sim$0.2−0.4 km s^{-1}, e.g., $H^{13}CO^+$ (1−0)) and two wide SPWs ($\sim$1.8 GHz) with spectral resolution of $\sim$1.6 km s^{-1}.

The QUARKS survey is a follow-up to the ATOMS survey, which observed 139 massive star-forming protocluster clumps through 156 single-pointings. QUARKS observations were obtained with three different ALMA configurations at Band 6 ($\sim$1.3 mm), including relatively low ($\sim$5″), moderate ($\sim$1″), and high ($\sim$0.″3) angular resolution, which were performed using the ACA 7 m array, the ALMA 12 m compact array C-2 (TM2) and extended C-5 (TM1) configurations, respectively. More details regarding the QUARKS survey are available in X. Liu et al. (2024), F. Xu et al. (2024b), and D. Yang et al. (2025). Combining three configuration observations from the QUARKS survey for both continuum and line data yielded a synthesized beam size of $\sim$0.″3. The combined QUARKS continuum data of the I18290 region have a typical sensitivity of rms ($\sigma_{1.3\ \mathrm{mm}}$) $\sim$0.14 mJy beam^{-1}. Four SPWs were configured for the QUARKS survey, with a bandwidth of $\sim$1.8 GHz and a velocity resolution of $\sim$1.3 km s^{-1} for each SPW.

3. Results

3.1. Parameter Estimation of Core and Condensation

To ensure consistent parameter estimation, the *imfit* task in *CASA* (CASA Team et al. 2022) was used to extract structures from both ATOMS 3 mm and QUARKS 1.3 mm dust continuum maps. The *imfit* task involves a two-dimensional Gaussian fit to the continuum emission of structures. We adopt a hierarchical terminology by designating ATOMS-identified structures as cores and QUARKS-resolved substructures as condensations (see Figure 2). Note that these terms represent manifestations of the same structure at different spatial resolutions. Only a single compact condensation is observed in the core C2 (see Figure 2(b)), indicating that the cloud core has not undergone fragmentation at the high angular resolution ($\sim$0.″3) of the QUARKS survey. The observed parameters of the core and the condensation retrieved with the *imfit* task are listed in Table 1.

If we assume that the 3 and 1.3 mm continuum emission is optically thin and mainly arises from thermal dust radiation, the masses of the core and condensation can be estimated using the following expression:

$$M_{\mathrm{gas}} = \frac{R_{\mathrm{gd}} S_{\nu}^{\mathrm{int}} D^2}{\kappa_{\nu} B_{\nu}(T_{\mathrm{dust}})}, \quad (1)$$

where R_{gd} is the ratio of gas to dust (assumed to be 100), S_{ν}^{int} is the integrated flux derived, and D is the distance to the source. The dust opacity, κ_{ν}, is taken as 0.18 and 0.9 cm^2 g^{-1} for the 3 and 1.3 mm continuum emission, respectively (V. Ossenkopf & T. Henning 1994). $B_{\nu}(T_{\mathrm{dust}})$ is the Planck function at a given dust temperature.

Dust temperatures as low as 10–15 K have been reported in several IRDC environments harboring starless cores without internal protostellar heating (P. Sanhueza et al. 2013; A. T. Barnes et al. 2023; X. Mai et al. 2024). In this case, given the starless nature of the C2 core (see Section 3.2), we adopt 10 K as the lower limit for the dust temperature. Further, the average dust temperature of the natal clump (22 K, derived from the spectral energy distribution; J. S. Urquhart et al. 2018) is considered as the upper limit. For these temperature limits, the estimated masses of the C2 core and condensation are 26.9–68.2 $M_{\odot}$ and 6.1–19.1 $M_{\odot}$ at 3 and 1.3 mm, respectively.

In addition, assuming a spherical geometry, the average number density can be calculated as $n_{\mathrm{H_2}} = \frac{3M_{\mathrm{core}}}{4\pi R_{\mathrm{c}}^3 \mu m_{\mathrm{H}}}$, where $\mu = 2.8$ is the mean molecular weight of the hydrogen molecule, and m_{H} is the mass of the hydrogen atom (J. Kauffmann et al. 2008). The effective radius, R_{c}, is estimated as $\sqrt{\mathrm{FWHM}_{\mathrm{maj}}^{\mathrm{Decon}} \times \mathrm{FWHM}_{\mathrm{min}}^{\mathrm{Decon}}}/2 \times D$, where $\mathrm{FWHM}_{\mathrm{maj}}^{\mathrm{Decon}}$ and $\mathrm{FWHM}_{\mathrm{min}}^{\mathrm{Decon}}$ are the deconvolved FWHM of the major and minor axes, respectively (see columns (7)–(8) in Table 1). The radii of the C2 core and condensation are $\sim$2800 $\pm$ 500 au and $\sim$400 $\pm$ 20 au, respectively. The average number densities are $0.4-1.0 \times 10^8$ cm^{-3} and $2.6-7.9 \times 10^9$ cm^{-3}, respectively. The estimated physical parameters of the core and condensation are listed in Table 2.

3.2. Evolutionary Stage of the C2 Core

Starless cores lack any star formation signatures, such as outflows traced by CO emission (e.g., A. Y. Yang et al. 2018, 2022; P. Sanhueza et al. 2019; J. S. Urquhart et al. 2022). We present the averaged spectra obtained from the ATOMS (two SPWs) and QUARKS (four SPWs) surveys for the C2 core and condensation in Figures 3(a) and (b), respectively. Molecular line emission of HC_3N is detected in the ATOMS SPW2 spectrum. The QUARKS spectra exhibit ^{13}CO (2–1), CO (2–1), and H_2CO ($3_{0,3}$–$2_{0,2}$) molecular lines. Additionally, N_2D^+ (3–2) emission is marginally detected with a low signal-to-noise ratio, which can be confirmed in the zoom-in image of the detected spectral lines in Figure 3(c) (see more in Section 3.3).

S. Zhang et al. (2023) used SiO and HCO^+ emission from the ATOMS survey to search for outflows in the I18290 region, concluding that no outflows were detected toward the massive core C2. To confirm this result, we analyze the CO (2–1) emission from the QUARKS survey, which provides

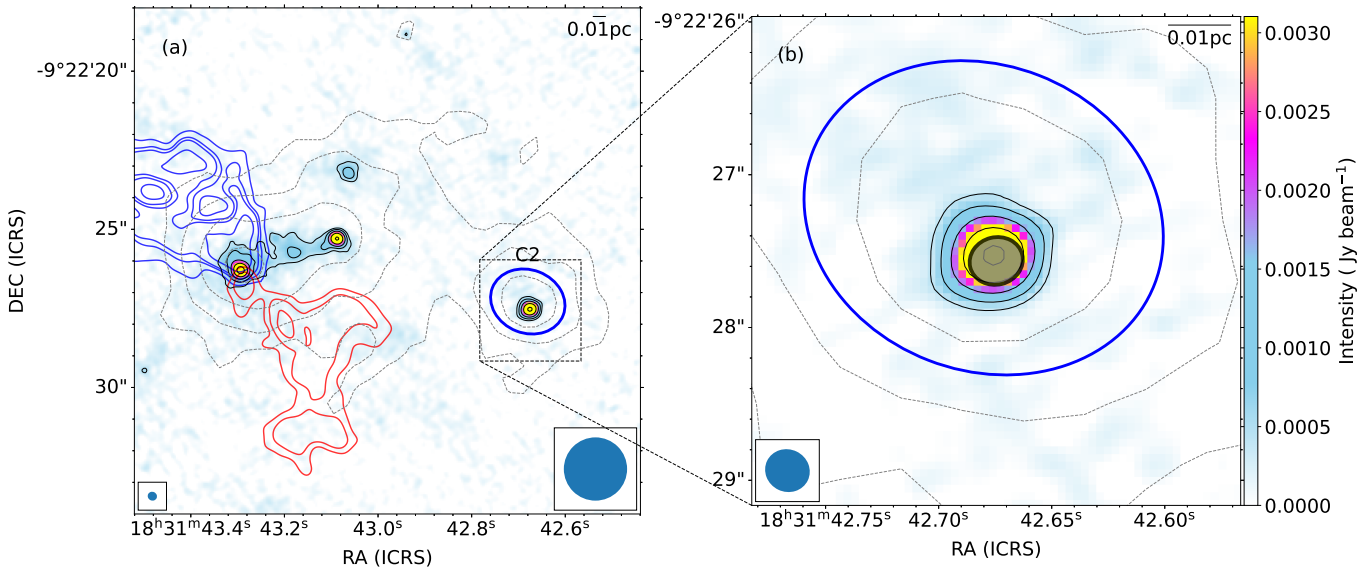

Figure 2. QUARKS 1.3 mm dust continuum image (color scale) overlaid with ATOMS 3 mm dust continuum emission (in gray dashed contours, identical to those in Figure 1). The black contours are at levels of [3, 6, 12, 24, 48] × $\sigma_{1.3\ \mathrm{mm}}$, with $\sigma_{1.3\ \mathrm{mm}} \sim$ 0.14 mJy beam^{-1}. The blue ellipses correspond to the FWHM sizes of the C2 core estimated from the ATOMS 3 mm image using the task *CASA imfit*. The synthesized beam sizes of the QUARKS and ATOMS survey are shown in the left and right bottom (panel (a)), respectively. The 0.01 pc scale bar is shown in the upper right corner. Panel (a): CO (2–1) outflow is overlaid on the QUARKS 1.3 mm dust continuum map. The blue and red contour levels are [3, 6, 12, 24, 48] × σ_{co}, with $\sigma_{\mathrm{co}} \sim$ 0.08 Jy beam^{-1} km s^{-1} for the blue lobes and ∼0.06 Jy beam^{-1} km s^{-1} for the red lobes. The corresponding velocity ranges are plus/minus 5−30 km s^{-1} relative to V_{LSR} (∼84.5 km s^{-1}) of the C2 core. Panel (b): zoom-in view of the C2 core. The black ellipses correspond to the FWHM sizes of the condensation estimated from the QUARKS 1.3 mm image using the task *CASA imfit*.

enhanced resolution to investigate potential outflows in this region. The CO line profile is integrated in a velocity range of 5−30 km s^{-1} relative to the systemic velocity (∼84.5 km s^{-1}), and the spatial distribution is shown by the blue and red contours in Figure 2(a). No CO outflow is detected toward the massive core C2 in the I18290 region. In a recent study based on ATOMS data, A. Hoque et al. (2025) proposed the HC_3N transition as an effective tracer of low-velocity components of outflows. They reported the detection of an outflow associated with the I18290 region. A careful inspection of Figure A1 in A. Hoque et al. (2025) confirms that the identified outflow is not associated with the C2 core. Furthermore, no line wings were identified in the H_2CO ($3_{0,3}$–$2_{0,2}$) transition, which is also considered as an outflow tracer (X. Liu et al. 2024). The absence of the outflow signature in the line transitions investigated is consistent with the findings of S. Zhang et al. (2023). In addition, weak detection of the N_2D^+ line toward the C2 core indicates the presence of cold dense gas (A. Crapsi et al. 2005; X. Liu et al. 2024). Due to the spatial filtering-out effect of the interferometric observations, it is likely that the detected N_2D^+ line emission probes the C2 core rather than the extended envelope. Therefore, this evidence of the cold dense gas, coupled with the absence of detected outflows, supports the starless nature of the C2 core.

3.3. Dynamical Stability of C2 Core and Condensation

Understanding the stability of the unfragmented C2 core against gravitational collapse is essential for assessing the potential formation of a high-mass star in this core. This can be assessed by estimating the virial parameters (α_{vir}), which, for an ideal spherical structure of uniform density, is given by (F. Bertoldi & C. F. McKee 1992; S. Dib et al. 2007)

$$\alpha_{\mathrm{vir}} = \frac{5\sigma_{\mathrm{eff}}^2 R_c}{G M_c}, \quad (2)$$

where σ_{eff} is the effective sound speed. R_c and M_c are the radius and mass of the structure, respectively. σ_{eff} can be substituted by the total velocity dispersion ($\sigma_{\mathrm{tot}}^2 = \sigma_{\mathrm{th}}^2 + \sigma_{\mathrm{nt}}^2$). The thermal velocity dispersion is $\sigma_{\mathrm{th}} = \sqrt{k_B T/\mu_p m_H}$, where $\mu_p = 2.33$ is the mean molecular weight per free particle (J. Kauffmann et al. 2008). In this study, the molecular line emission of $H^{13}CO^+$ (1−0) from the ATOMS survey and N_{2D}^+ (3–2) from the QUARKS survey were used to estimate the contribution of nonthermal motion from turbulence to the C2 core and condensation, respectively. The ATOMS $H^{13}CO^+$ (1−0) line emission provides high velocity resolution (∼0.2 km s^{-1}) and is a probe typical of dense core envelopes (e.g., $n_{\mathrm{crit}} \sim 10^5$ cm^{-3}; T. Gerner et al. 2014). In contrast, for the higher angular resolution QUARKS data, N_{2D}^+ (3–2) line emission was adopted to serve as kinematic tracers for colder and denser conditions (A. Crapsi et al. 2005, 2007). Despite the low signal-to-noise ratio, marginal detection of N_2D^+ emission is confirmed by cross-checking with other detected molecular lines of the C2 core (see Figure 3). The nonthermal velocity dispersion is $\sigma_{\mathrm{nt}} = \left(\sigma_{\mathrm{line}}^2 - \frac{k_B T}{m_{\mathrm{line}}}\right)^{1/2}$, where k_B is the Boltzmann constant and m_{line} is the molecular mass of the observed molecule ($m_{\mathrm{line}} = 30 m_H$ for the $H^{13}CO^+$ line and $m_{\mathrm{line}} = 32 m_H$ for N_2D^+). The observed dispersions (σ_{obs}) are ∼0.62 km s^{-1} for $H^{13}CO^+$ of the C2 core and ∼0.50 km s^{-1} for N_2D^+ of condensation, as shown in Figure 4.

The total velocity dispersion is estimated to be ∼0.65 km s^{-1} for $H^{13}CO^+$ and ∼0.53 km s^{-1} for N_2D^+. From

Table 1
Observed Parameters of Core and Condensation from *CASA imfit*

Source	R.A. (ICRS)	Decl. (ICRS)	$\mathrm{FWHM_{maj}}$ (arcsec)	$\mathrm{FWHM_{min}}$ (arcsec)	PA (deg)	$\mathrm{FWHM_{maj}^{Decon}}$ (arcsec)	$\mathrm{FWHM_{min}^{Decon}}$ (arcsec)	F_ν^{int} (mJy)	F_ν^{peak} (mJy beam^{-1})	Data
(1)	(2)	(3)	(4)	(5)	(6)	(7)	(8)	(9)	(10)	(11)
Core	18:31:42.68	−09:22:27.28	2.4 ± 0.1	2.0 ± 0.1	68.8 ± 8.8	1.2 ± 0.3	0.9 ± 0.3	2.15 ± 0.13	1.66 ± 0.06	Band3
Condensation	18:31:42.67	−09:22:27.53	0.35 ± 0.01	0.31 ± 0.01	103.9 ± 3.8	0.21 ± 0.01	0.12 ± 0.01	11.21 ± 0.22	8.35 ± 0.11	Band6

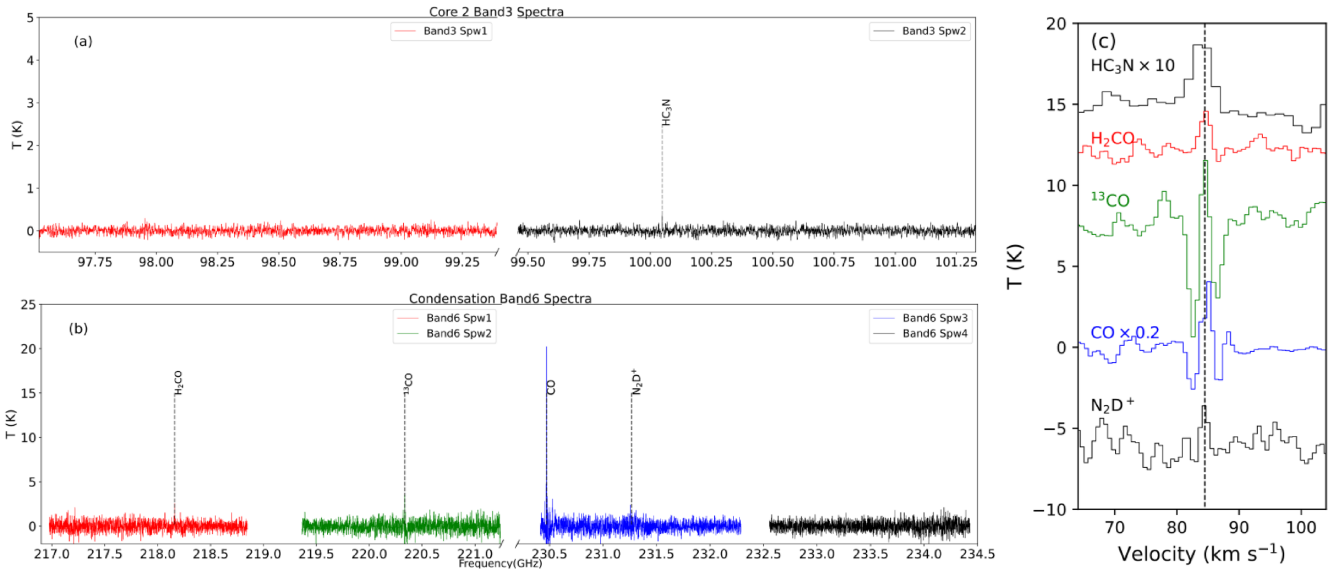

Figure 3. Average spectra of the C2 core/condensation. (a): average spectra extracted from two ATOMS wideband SPWs over the C2 core. (b): same as panel (a) but for four QUARKS SPWs over the C2 condensation. (c): zoom-in view of the molecular lines detected in the six SPWs (corresponding to panels (a) and (b)). The dashed line indicates the systemic velocity of the C2 core (∼84.5 km s^{-1}). Note that the absorption dips present in both ^{13}CO and CO spectra are artifacts arising from the missing flux by ALMA, which will be addressed in future, more in-depth studies by combining our QUARKS data with new single-dish observations.

Table 2
Physical Parameters of the Core and Condensation

Source	Radius[a]	σ_{obs}	Temperature	Mass	n_{H_2}	α_{vir}	Data
G022.3501+00.0697	(au)	(km s^{-1})	(K)	($M_\odot$)	(10^8 cm^{-3})		
(1)	(2)	(3)	(4)	(5)	(6)	(7)	(8)
Core	2800 ± 500	0.62 ± 0.37	10	68.2 ± 13.4	0.9 ± 0.5	0.10 ± 0.03	Band 3
			22	26.9 ± 5.2	0.4 ± 0.2	0.27 ± 0.09	
Condensation	400 ± 50	0.50 ± 0.20	10	19.1 ± 3.6	79.0 ± 20.0	0.03 ± 0.01	Band 6
			22	6.1 ± 1.2	25.5 ± 6.5	0.12 ± 0.04	

Note.
[a] Beam-dencovolved.

these values, we calculate α_{vir} to be ∼0.1–0.3 for both the C2 core and the condensation, in the temperature range of 10–22 K. Following Equation (5) of T. Pillai et al. (2011) with the magnetic field contribution is considered, such low values of $\alpha_{vir} \ll 1$ are possible in the case of magnetized cloud fragments, provided the magnetic field is strong ∼1 mG (J. Kauffmann et al. 2013). Recent observational measurements using the Davis–Chandrasekhar–Fermi method do yield field strengths of 1–10 mG in massive star-forming regions (e.g., P. C. Cortés et al. 2021; J. Hwang et al. 2021, 2022, 2025; P. Saha et al. 2024; L. A. Zapata et al. 2024; P. Sanhueza et al. 2025), and smaller values of ∼0.1−1 mG in starless/prestellar core (J. M. Kirk et al. 2006; J. Karoly et al. 2020; K. Pattle et al. 2021; J. Hwang et al. 2023).

The stability analysis is consistent with the observed fragmentation scenario of the C2 core, where only a single smaller-scale condensation is detected. Several theoretical and numerical studies suggest that magnetic fields, by providing support against gravity, play a key role in suppressing fragmentation. In a recent study, A. Palau et al. (2021) studied 18 massive dense cores to investigate this correlation. Though not robustly observed, these authors discuss the possible influence of the magnetic field on the fragmentation process. Based on the above arguments, one can infer C2 core to be an unfragmented, massive, and subvirial entity in a strong magnetized environment. This core is therefore gravitationally bound and has the potential to collapse toward star formation.

4. Discussion and Conclusions

Despite the fact that F. Motte et al. (2018) have proposed an evolutionary scheme for high-mass stars that excludes the massive prestellar phase, the empirical identification of several high-mass prestellar cores provides strong evidence for their existence. There are several examples from the previous literature. A. Duarte-Cabral et al. (2013) reported the detection of a high-mass prestellar core candidate (CygX-N53-MM2) with a mass of ∼21 $M_\odot$ and a radius of 2500 au, which may be, however, associated with tentative outflows. K. Wang et al. (2014) have also observed a candidate (i.e., G11.11-P6-SMA1; mass of ∼28 $M_\odot$ and radius of ∼2000 au) without any signatures of CO outflows in SMA observations. However, this source has yet to be confirmed by higher-angular-resolution ALMA observations. In the ALMA-Initial Mass Function Large Program, M. Valeille-Manet et al. (2025) identified 12 prestellar cores of masses greater than 16 $M_\odot$, 4 of which are above 30 $M_\odot$. These sources have no associated CO and/or SiO outflows detected. However, a comprehensive survey of molecular lines with sufficiently broad bandwidths has not

been conducted for these massive candidates, which is vital for accurately classifying prestellar cores. For instance, detection of COMs, such as CH_3OH, in the 4.8 GHz SPWs of the high-mass prestellar core candidate W43-MM1, typically linked with hot cores, raises questions about its classification. This suggests that W43-MM1 is more likely in the early protostellar phase rather than a high-mass prestellar core candidate (T. Nony et al. 2018; J. Molet et al. 2019). In addition, albeit with an examination of a wide-ranging molecular line survey, the classification of several other massive prestellar core candidates remains uncertain. This includes C2c1a (A. T. Barnes et al. 2023) and MM1-C and MM1-E1 (X. Mai et al. 2024). For example, C2c1a is linked with faint CO outflows, as depicted in Figure 3 of A. T. Barnes et al. (2023), suggesting the beginning of protostellar activity. Additionally, high-resolution imaging of MM1-C indicates fragmentation (X. Mai et al. 2024), questioning its classification as a singular high-mass prestellar core.

In this study, we present the C2 core in the I18290 massive star-forming region as a prestellar core candidate, based on ALMA two-band observations from the ATOMS and QUARKS surveys. Under the assumption of a 10 K dust temperature, we estimate the physical parameters of the C2 core using 3 mm dust continuum emission from the ATOMS survey. The mass, radius, and average number density of the core were estimated to be ~27–68 $M_\odot$, ~2800 au, and ~10^8 cm^{-3}, respectively. In striking contrast to the clustered, centrally located environment of the 12 massive prestellar cores reported by M. Valeille-Manet et al. (2025), it is worth noting that the C2 core is rather isolated. Subsequent higher-angular-resolution (~0.″3) 1.3 mm dust continuum data from the QUARKS survey revealed that the C2 core remains unfragmented, hosting only a central compact condensation with a mass of ~19 $M_\odot$, a radius of ~400 au, and an average number density of ~10^9 cm^{-3}. This condensation exhibits highly compact dust emission with nearly circular symmetry (ellipticity ~1.1) (see Figure 2). Including the results from S. Zhang et al. (2023), no outflows (tracers, HCO^+, SiO, and CO) were detected, nor was any young stellar object identified (see Section 4.2 in S. Zhang et al. 2023) with the massive C2 core. Furthermore, we only detected six molecular line emissions within six SPWs (two from the ATOMS survey, ~4 GHz; four from the QUARKS survey, ~8 GHz; see Figure 3). None of the detected molecular line transitions are tracers of dense warm gas. Our stability analysis reveals that thermal and turbulent support alone is insufficient to counteract gravitational collapse, giving a virial parameter of ~0.1−0.3. These low values of the virial parameter suggest a strong magnetized environment, which lends further support to the unfragmented nature of the C2 core.

The identification of the C2 core in I18290 presents a case study in support of the turbulent core model. The influence of environment leading to core mass growth can be ruled out—the more evolved the natal environment, the more massive the embedded core. Though associated with the BRC I18290, the C2 core is located in an IR-dark lane (see Figure 1), strongly indicating its very early evolutionary stage and its massive nature from the beginning. Additionally, the isolated nature of the C2 prestellar candidate provides a template for more in-depth studies, such as modeling and chemical evolution analysis. Although our study has outlined its fundamental physical properties, a conclusive classification also hinges on the chemical evolution analysis. Our upcoming investigations aim to determine the chemical nature of this prestellar core candidate through quantitative analysis of molecular abundances and comparisons with chemical models, with an emphasis on the elevated abundances of deuterated isotopologues (e.g., P. Caselli et al. 1999, 2022; A. Crapsi et al. 2005).

Acknowledgments

This work has been supported by the National Key R&D Program of China (No. 2022YFA1603101), the National Natural Science Foundation of China (NSFC) through grant Nos. 12073061, 12122307, and 12033005. H.-L.L. is supported by Yunnan Fundamental Research Project (grant Nos. 202301AT070118 and 202401AS070121), and by Xingdian Talent Support Plan—Youth Project. D.-T.Y. is supported by the Scientific Research Fund Project of Yunnan Education Department (Project ID: 2025Y0106, KC-24248416). T.L. acknowledges the support by the PIFI program of Chinese Academy of Sciences through grant No. 2025PG0009, and the Tianchi Talent Program of Xinjiang Uygur Autonomous Region. G.G. gratefully acknowledges support by the ANID BASAL project FB210003. P.S. was partially supported by a Grant-in-Aid for Scientific Research (KAKENHI No. JP23H01221) of JSPS. This work was performed in part at the Jet Propulsion Laboratory, California Institute of Technology, under contract with the National Aeronautics and Space Administration (80NM0018D0004). S.R.D. acknowledges support from the Fondecyt Postdoctoral fellowship (project code 3220162) and ANID BASAL project FB210003. This work is sponsored (in part) by the Chinese Academy of Sciences (CAS), through a grant to the CAS South America Center for Astronomy (CASSACA) in Santiago, Chile. L.Z., P.G., and J.H. are supported by Chinese Academy of Sciences South America Center for Astronomy (CASSACA) Key Research Project E52H540201 and the China-Chile Joint Research Fund (CCJRF 2211). CCJRF is provided by the CASSACA and established by National Astronomical Observatories, Chinese Academy of Sciences (NAOC), and Chilean Astronomy Society (SOCHIAS) to support China-Chile collaborations in astronomy. L.B. gratefully acknowledges support by the ANID BASAL project FB210003. This paper makes use of the following ALMA data: ADS/JAO.ALMA#2019.1.00685.S and ADS/JAO.ALMA#2021.1.00095.S.

Appendix

Gaussian fitting of the average spectra of $H^{13}CO^+$ molecular emission from the C2 core using the ATOMS data (see Figure 4a) and N_2D^+ molecular emission from the condensation using the QUARKS data (see Figure 4b).

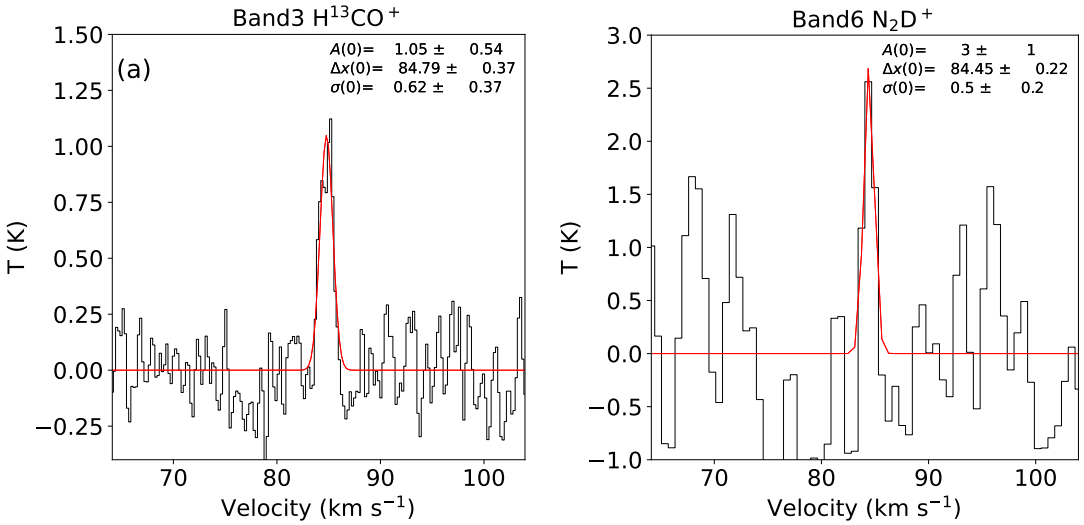

Figure 4. Average spectra of $H^{13}CO^+$ from the ATOMS survey and average spectra of N_2D^+ from the QUARKS survey.

ORCID iDs

Dongting Yang https://orcid.org/0009-0004-6159-5375
Hong-Li Liu https://orcid.org/0000-0003-3343-9645
Sheng-li Qin https://orcid.org/0000-0003-2302-0613
Tie Liu https://orcid.org/0000-0002-5286-2564
Anandmayee Tej https://orcid.org/0000-0001-5917-5751
Siju Zhang https://orcid.org/0000-0002-9836-0279
Xunchuan Liu https://orcid.org/0000-0001-8315-4248
Fengwei Xu https://orcid.org/0000-0001-5950-1932
Guido Garay https://orcid.org/0000-0003-1649-7958
Patricio Sanhueza https://orcid.org/0000-0002-7125-7685
Xiaofeng Mai https://orcid.org/0000-0001-7573-0145
Wenyu Jiao https://orcid.org/0000-0001-9822-7817
Paul F. Goldsmith https://orcid.org/0000-0002-6622-8396
Sami Dib https://orcid.org/0000-0002-8697-9808
Pablo García https://orcid.org/0000-0002-8586-6721
Di Li https://orcid.org/0000-0003-3010-7661
Jinhua He https://orcid.org/0000-0002-3938-4393
A. Y. Yang https://orcid.org/0000-0003-4546-2623
Prasanta Gorai https://orcid.org/0000-0003-1602-6849
Suinan Zhang https://orcid.org/0000-0002-8389-6695
Mika Juvela https://orcid.org/0000-0002-5809-4834
James O. Chibueze https://orcid.org/0000-0002-9875-7436
Chang Won Lee https://orcid.org/0000-0002-3179-6334
Jihye Hwang https://orcid.org/0000-0001-7866-2686
Leonardo Bronfman https://orcid.org/0000-0002-9574-8454
Xindi Tang https://orcid.org/0000-0002-4154-4309
Archana Soam https://orcid.org/0000-0002-6386-2906
Tapas Baug https://orcid.org/0000-0003-0295-6586
Swagat Ranjan Das https://orcid.org/0000-0002-3658-0516
L. K. Dewangan https://orcid.org/0000-0001-6725-0483
L. Viktor Tóth https://orcid.org/0000-0002-5310-4212

References

Andre, P., Ward-Thompson, D., & Barsony, M. 2000, in Protostars and Planets IV, ed. V. Mannings, A. P. Boss, & S. S. Russell (Univ. Arizona Press), 59
Barnes, A. T., Liu, J., Zhang, Q., et al. 2023, A&A, 675, A53
Bertoldi, F., & McKee, C. F. 1992, ApJ, 395, 140
Beuther, H., Mottram, J. C., Ahmadi, A., et al. 2018, A&A, 617, A100
Bonnell, I. A., Bate, M. R., Clarke, C. J., & Pringle, J. E. 2001, MNRAS, 323, 785
Bontemps, S., Motte, F., Csengeri, T., & Schneider, N. 2010, A&A, 524, A18
CASA Team, Bean, B., Bhatnagar, S., et al. 2022, PASP, 134, 114501
Caselli, P., Pineda, J. E., Sipilä, O., et al. 2022, ApJ, 929, 13
Caselli, P., Walmsley, C. M., Tafalla, M., Dore, L., & Myers, P. C. 1999, ApJL, 523, L165
Coletta, A., Molinari, S., Schisano, E., et al. 2025, A&A, 696, A151
Cortés, P. C., Sanhueza, P., Houde, M., et al. 2021, ApJ, 923, 204
Crapsi, A., Caselli, P., Walmsley, M. C., & Tafalla, M. 2007, A&A, 470, 221
Crapsi, A., Caselli, P., Walmsley, C. M., et al. 2005, ApJ, 619, 379
Cyganowski, C. J., Brogan, C. L., Hunter, T. R., et al. 2014, ApJL, 796, L2
Das, S. R., Merello, M., Bronfman, L., et al. 2024, MNRAS, 534, 3832
Dib, S., Kim, J., Vázquez-Semadeni, E., Burkert, A., & Shadmehri, M. 2007, ApJ, 661, 262
Duarte-Cabral, A., Bontemps, S., Motte, F., et al. 2013, A&A, 558, A125
Gerner, T., Beuther, H., Semenov, D., et al. 2014, A&A, 563, A97
Hoque, A., Baug, T., Dewangan, L. K., et al. 2025, ApJ, 987, 197
Hwang, J., Kim, J., Pattle, K., et al. 2021, ApJ, 913, 85
Hwang, J., Kim, J., Pattle, K., et al. 2022, ApJ, 941, 51
Hwang, J., Pattle, K., Lee, C. W., et al. 2025, ApJ, 985, 222
Hwang, J., Pattle, K., Parsons, H., Go, M., & Kim, J. 2023, AJ, 165, 198
Jiao, W., Wang, K., Pillai, T. G. S., et al. 2023, ApJ, 945, 81
Karoly, J., Soam, A., Andersson, B. G., et al. 2020, ApJ, 900, 181
Kauffmann, J., Bertoldi, F., Bourke, T. L., Evans, N. J., II, & Lee, C. W. 2008, A&A, 487, 993
Kauffmann, J., Pillai, T., & Goldsmith, P. F. 2013, ApJ, 779, 185
Kirk, J. M., Ward-Thompson, D., & Crutcher, R. M. 2006, MNRAS, 369, 1445
Lada, C. J., & Lada, E. A. 2003, ARA&A, 41, 57
Liu, H.-L., Liu, T., Evans, N. J., II, et al. 2021, MNRAS, 505, 2801
Liu, T., Evans, N. J., Kim, K.-T., et al. 2020, MNRAS, 496, 2790
Liu, X., Liu, T., Zhu, L., et al. 2024, RAA, 24, 025009
Louvet, F., Neupane, S., Garay, G., et al. 2019, A&A, 622, A99
Lu, X., Zhang, Q., Liu, H. B., Wang, J., & Gu, Q. 2014, ApJ, 790, 84
Mai, X., Liu, T., Liu, X., et al. 2024, ApJL, 961, L35
McKee, C. F., & Tan, J. C. 2003, ApJ, 585, 850
Mège, P., Russeil, D., Zavagno, A., et al. 2021, A&A, 646, A74
Molet, J., Brouillet, N., Nony, T., et al. 2019, A&A, 626, A132
Morii, K., Sanhueza, P., Nakamura, F., et al. 2023, ApJ, 950, 148
Morii, K., Sanhueza, P., Zhang, Q., et al. 2024, ApJ, 966, 171
Motte, F., Bontemps, S., & Louvet, F. 2018, ARA&A, 56, 41
Motte, F., Bontemps, S., Schilke, P., et al. 2007, A&A, 476, 1243
Nony, T., Louvet, F., Motte, F., et al. 2018, A&A, 618, L5
Ossenkopf, V., & Henning, T. 1994, A&A, 291, 943
Padoan, P., Pan, L., Juvela, M., Haugbølle, T., & Nordlund, Å. 2020, ApJ, 900, 82
Palau, A., Zhang, Q., Girart, J. M., et al. 2021, ApJ, 912, 159
Pattle, K., Lai, S.-P., Di Francesco, J., et al. 2021, ApJ, 907, 88
Peretto, N., Fuller, G. A., Duarte-Cabral, A., et al. 2013, A&A, 555, A112
Pillai, T., Kauffmann, J., Wyrowski, F., et al. 2011, A&A, 530, A118
Saha, P., Sanhueza, P., Padovani, M., et al. 2024, ApJL, 972, L6
Sanhueza, P., Contreras, Y., Wu, B., et al. 2019, ApJ, 886, 102
Sanhueza, P., Jackson, J. M., Foster, J. B., et al. 2013, ApJ, 773, 123

Sanhueza, P., Jackson, J. M., Zhang, Q., et al. 2017, ApJ, 841, 97
Sanhueza, P., Liu, J., Morii, K., et al. 2025, ApJ, 980, 87
Sugitani, K., Fukui, Y., & Ogura, K. 1991, ApJS, 77, 59
Sugitani, K., & Ogura, K. 1994, ApJS, 92, 163
Svoboda, B. E., Shirley, Y. L., Traficante, A., et al. 2019, ApJ, 886, 36
Tan, J. C., Kong, S., Butler, M. J., Caselli, P., & Fontani, F. 2013, ApJ, 779, 96
Urquhart, J. S., König, C., Giannetti, A., et al. 2018, MNRAS, 473, 1059
Urquhart, J. S., Wells, M. R. A., Pillai, T., et al. 2022, MNRAS, 510, 3389
Valeille-Manet, M., Bontemps, S., Csengeri, T., et al. 2025, A&A, 696, A11
Vázquez-Semadeni, E., Palau, A., Ballesteros-Paredes, J., Gómez, G. C., & Zamora-Avilés, M. 2019, MNRAS, 490, 3061
Wang, K., Zhang, Q., Testi, L., et al. 2014, MNRAS, 439, 3275
Xu, F., Wang, K., Liu, T., et al. 2024a, ApJS, 270, 9
Xu, F., Wang, K., Liu, T., et al. 2024b, RAA, 24, 065011
Yang, A. Y., Thompson, M. A., Urquhart, J. S., & Tian, W. W. 2018, ApJS, 235, 3
Yang, A. Y., Urquhart, J. S., Wyrowski, F., et al. 2022, A&A, 658, A160
Yang, D., Liu, H.-L., Liu, T., et al. 2025, ApJS, 280, 33
Yang, D., Liu, H.-L., Tej, A., et al. 2023, ApJ, 953, 40
Zapata, L. A., Fernández-López, M., Sanhueza, P., et al. 2024, ApJ, 974, 257
Zhang, Q., Wang, K., Lu, X., & Jiménez-Serra, I. 2015, ApJ, 804, 141
Zhang, Q., Wang, Y., Pillai, T., & Rathborne, J. 2009, ApJ, 696, 268
Zhang, S., Wang, K., Liu, T., et al. 2023, MNRAS, 520, 322
Zhang, S., Zavagno, A., López-Sepulcre, A., et al. 2021, A&A, 646, A25